Supporting Information

Cobalt phosphosulfide in tetragonal phase: highly active and durable catalyst for hydrogen evolution reaction

Jinfa Chang[a,c,d], Yixin Ouyang[b], Junjie Ge [a,]*, Jinlan Wang [b,]*, Changpeng Liu[a] and Wei Xing [a,]*

[a] State Key Laboratory of Electroanalytica Chemistry, Jilin Province Key Laboratory of Low Carbon Chemical Power, Changchun Institute of Applied Chemistry, Chinese Academy of Sciences, Changchun 130022, PR China. E-mail: xingwei@ciac.ac.cn; gejj@ciac.ac.cn

[b] School of Physics, Southeast University, Nanjing 211189, PR, China. E-mail: jlwang@seu.edu.cn

[c] Research Institute of Electrochemical Energy, National Institute of Advanced Industrial Science and Technology (AIST), Ikeda, Osaka 563-8577, Japan.

[d] AIST-Kyoto University Chemical Energy Materials Open Innovation Laboratory (ChEM-OIL), Yoshida, Sakyo-ku, Kyoto 606-8501, Japan.

Experimental Section

Materials

Carbon paper (CP, #60, Fuel Cell Earth http://www.fuelcellstore.com/toray-carbon-paper-060?search=TGP) was provided by Fuel Cell Store (USA), with the thickness of 0.19 mm, the electrical resistivity in through plane is 80 mΩ cm and in plane is 5.8 mΩ cm, the specific surface area is 82.52 m^2 g^{-1}. Pt/C (20 wt% Pt on Vulcan XC-72R, Johnson Matthey Company, HiSPEC™ 3000), Co(ac)$_2$·4H$_2$O, NH$_4$F, (NH$_2$)$_2$CO, NaH$_2$PO$_2$·H$_2$O and sulphur power was purchased from Sigma-Aldrich Chemical Reagent Co., Ltd., (USA). All the reagents were used as received. Highly purified nitrogen ($\geq$ 99.99%) and Ar ($\geq$ 99.99%) were supplied by Changchun Juyang Co Ltd. The water used throughout all experiments was purified through a Millipore system (resistivity: $\rho \geq$ 18 MΩ cm).

Methods

Synthesis of cobalt precursor nanoneedles on carbon paper. A piece of CP was washed with HNO$_3$, ethanol and deionized water several times to ensure the surface of the CP was well cleaned before use. 2.0 mmol of Co(ac)$_2$·4H$_2$O, 4 mmol NH$_4$F, and 10 mmol (NH$_2$)$_2$CO were dissolved in 35 ml of distilled water. Then, the above solution was transferred to a 50-ml PTFE-lined stainless steel autoclave containing the CP (1*1 cm^2), which was sealed and heated at 120 ℃ for 5 h. After cooling, the substrate was removed, rinsed with ethanol and water, and dried under a stream of nitrogen.

Synthesis of CoPS nanoneedles on carbon paper. An alumina boat containing 0.015 mol of a 1:1 mixture of sulphur powders and NaH$_2$PO$_2$·H$_2$O was covered with a piece of glass, then placed in the center of a fused silica tube reactor equipped with gas flow controllers. The Co nanoneedles precursor substrates were placed on an alumina plate at the downstream end of the tube. The furnace was then heated to 500 ℃ with 2 ℃ min^{-1} for 1 h to convert these precursors to CoPS before the furnace was cooled down naturally under a static Ar atmosphere with a flow rate of 80 cc min^{-1}. After cooling, the products were rinsed with HCl, ethanol and water several times. The loading of CoPS on CP was determined as ~ 0.2 mg cm^{-2} using a high-precision microbalance. For comparison, CoPS with loading of ca. 0.1 mg cm^{-2} and 0.3 mg cm^{-2} was also prepared through adjust the content of precursor. Besides, a series of CoP$_x$S$_{2-x}$/C (x=0.5, 0.66, 1, 1.34 and 1.5; when x=1, CoPS/CP was obtained) with catalyst loading of ~0.2 mg cm^{-2} on carbon paper were also prepared through adjust the content of P and S precursor.

Synthesis of CoP and CoS₂ nanoneedles on carbon paper. The CoP and CoS_2 was synthesized through the same method to synthesized the CoPS, unless the sulphur powders or $NaH_2PO_2 \cdot H_2O$ is absent.

Physical characterizations

Scanning electron microscopy (SEM) measurements were performed with an XL 30 ESEM FEG field emission scanning electron microscope. Transmission electron microscopy (TEM), high resolution transmission electron microscopy (HR-TEM), high-annular dark-field scanning transmission electron microscopy (STEM) and element mapping analysis were conducted on Philips TECNAI G2 electron microscope operating at 200 kV. X-ray diffraction (XRD) measurements were performed with a PW-1700 diffractometer using a Cu K_α (λ=1.5405 Å) radiation source (Philips Co.). The textural and morphological features of the samples were determined by nitrogen physisorption at 77 K in a Micromeritics ASAP 2020. Textural properties such as the specific surface area pore volume and pore size distribution were calculated from each corresponding nitrogen adsorption−desorption isotherm, applying the Brunauer-Emmett-Teller (BET) equation and the Barrett-Joyner-Halenda (BJH). X-ray photoelectron spectroscopy (XPS) measurements were carried out on Mg K_α radiation source (Kratos XSAM-800 spectrometer). The bulk compositions were evaluated by inductively coupled plasma optical emission spectrometer (ICP-OES, X Series 2, Thermo Scientific USA). Raman spectra were collected on a J-Y T64000 Raman spectrometer with 532 nm wavelength incident laser light. To ensure homogeneity of the samples, three spectra were recorded from different spots on the sample.

Electrochemical measurements

Electrochemical measurements were performed with EG & G PARSTAT 4000 potentiostat/galvanostat (Princeton Applied Research Co., USA). A conventional one-component three-electrode cell was used, the CoPS/CP (CoPS loading on CP: ~0.2 mg cm^{-2}) or other catalyst supported on carbon paper was used as working electrode directly, a saturated calomel electrode (SCE, Hg/Hg_2Cl_2) was used as the reference electrode. Potentials were measured versus saturated calomel electrode (SCE) and are reported versus reversible hydrogen electrode (RHE). A graphite plate was used as the counter electrode to avoid contamination from dissolved Pt. During the electrochemical experiments, the electrolyte was stirred using a magnetic stirrer rotating at 300 rpm to remove in situ-emerged H_2 bubbles. The catalysts were activated by at least 20 CV scans till stabilization at a scan rate of 100 mV s^{-1}, the linear sweep voltammetry (LSV) with a scan rate of 5 mV s^{-1} was then performed. Ohmic drop was corrected using electrochemical impedance spectroscopy (EIS) methods according

to the equation: $E_a = E_b - IR_s$, where E_a is the overpotential after *I-R* correction, E_b is the overpotential before *I-R* correction, I is the corresponding current and R_s is the resistance of the system obtained from EIS plots as the first intercept of the main arc, all data have been corrected for 90% iR potential drop. EIS were recorded at the frequency range from 100 kHz to 0.1 Hz with 10 points per decade. The amplitude of the sinusoidal potential signal was 5 mV. The durability of samples was assessed through chronopotentiometry under a static current density of 10 mA cm^{-2} (or 100 mA cm^{-2}) for 100 hours and 3000 cycles continuous cyclic voltammetry from 0.2 V to -0.4 V with scan rate of 100 mV s^{-1}.

The generated gas was confirmed by gas chromatography analysis and measured quantitatively using a calibrated pressure sensor to monitor the pressure change in the anode compartment of a H-type electrolytic cell. The Faradaic efficiency was calculated by comparing the amount of measured hydrogen with calculated hydrogen generated at a constant oxidative current of 10 mA cm^{-2} in 0.5 M H$_2$SO$_4$ for at least 90 min electrolysis (assuming 100% FE). Pressure data during electrolysis were recorded using a CEM DT-8890 Differential Air Pressure Gauge Manometer Data Logger Meter Tester with a sampling interval of 1 point per second.

Two-electrode Cell performance evaluation

To evaluate the practical application of CoPS in water electrolysis reaction, the CoPS catalyst was grown carbon paper (1 cm * 1cm) with a CoPS loading of ~0.2 mg cm^{-2} and used as cathode electrode directly. For compare analysis, Pt/C (20 wt.%) was first dispersed in ethanol, and the suspension was loaded onto carbon paper (1 cm * 1 cm) with a loading of 0.2 mg cm^{-2} Pt/C on carbon paper.

Commercial state-of-art IrO$_2$ was used as anode catalyst which loaded onto titanium felt sheets. Prior to the use of carbon paper and titanium felt (Alfa Aesar, porosity 95%, purity 95%) as the catalyst support, the carbon paper and titanium felt sheets were pretreated in acetone and then ethanol for 1 hour each and were thoroughly rinsed with deionized water. The Pt/C and IrO$_2$ loadings were both 0.2 mg cm^{-2}. To ensure that the catalyst bound to the carbon paper and titanium felt sheet support, 150 mL of PTFE (10%) was dispersed on each electrode, and then the carbon paper and titanium felt sheet was maintained at 250 °C for 1 hour. The LSV experiments were performed across a potential window from -2.0 to 2.0 V at a scan rate of 5 mV s^{-1} in 0.5 M H$_2$SO$_4$ or 1 M KOH. The stability of the electrolyzer was examined using galvanostatic experiments in the same electrolyte. The current density was kept constant at 100 mA cm^{-2} over 100 hours of elecltrolysis.

DFT Calculations

The spin-polarized DFT calculations were carried out within a general gradient approximation parametrized by Perdew, Burke, and Ernzerhof,[1] as implemented in Vienna ab initio simulation package.[2] The energy cutoff for the plane-wave basis set was set to be 400 eV. The convergence threshold was 10^{-4} eV for energy and 0.02 eV Å^{-1} for force, respectively. For calculations of adsorption energy, DFT simulations performed were based on the orthorhombic CoP (a=5.076 Å, b=3.277 Å, c=5.599 Å, JCPDS #65-2593, Figure S8a)[3], cubic CoS_2 (a=5.538 Å, JCPDS #41-1471, Figure S8b)[4] and tetragonal CoPS (space group P4, a=5.445 Å, c=5.457 Å, JCPDS #27-0139, Figure S8c), respectively. Chemisorption was modeled on the CoP (101), CoS_2 (100) and CoPS (100) surfaces. We adopted slabs with five CoS_2 layers consisting of 90 atoms ($Co_{30}S_{60}$) and five CoP layers consisting of 60 atoms ($Co_{30}P_{30}$). The periodically repeated slabs were separated from their neighboring images by a 10-Å-wide vacuum in the direction perpendicular to the surface. Further, we substituted 30 P atoms of CoS_2 for 30 S atoms to investigate the effects of P doping. The Gibbs free-energy (ΔG_{H*}) is expressed as:[5]

$$\Delta G_{H*} = \Delta E_{H*} + \Delta E_{ZPE} - T\Delta S$$

where Δ_{EH*} is the adsorption energy of atomic hydrogen on the given unit cell, ΔE_{ZPE} is the difference corresponding to the zero point energy between the adsorbed hydrogen and hydrogen in the gas phase and ΔS is entropy change of H* adsorption. As the entropy of hydrogen in absorbed state is negligible, ΔS can be calculated as -1/2 S_0 (S_0 is the entropy of H_2 in the gas phase at standard conditions, 1 bar of H_2 and pH = 0 at 300 K).
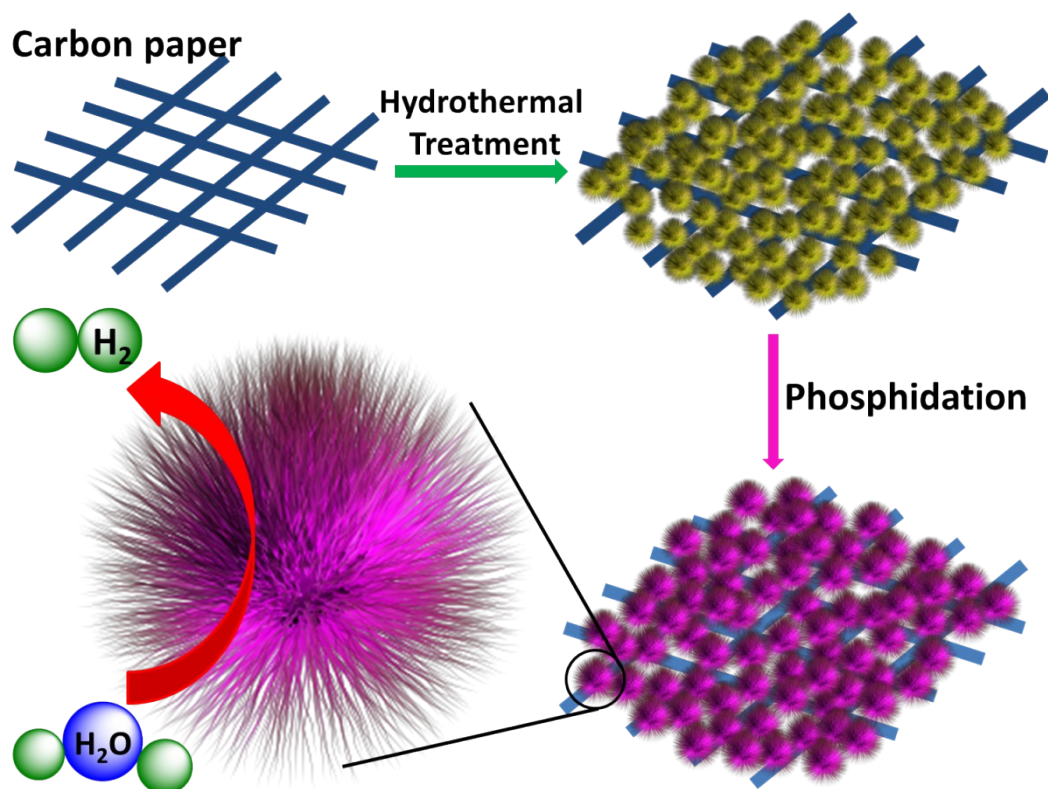
Scheme S1. Preparation process of the urchin like ternary CoPS nanoneedles used as efficient and robust catalysts for HER.
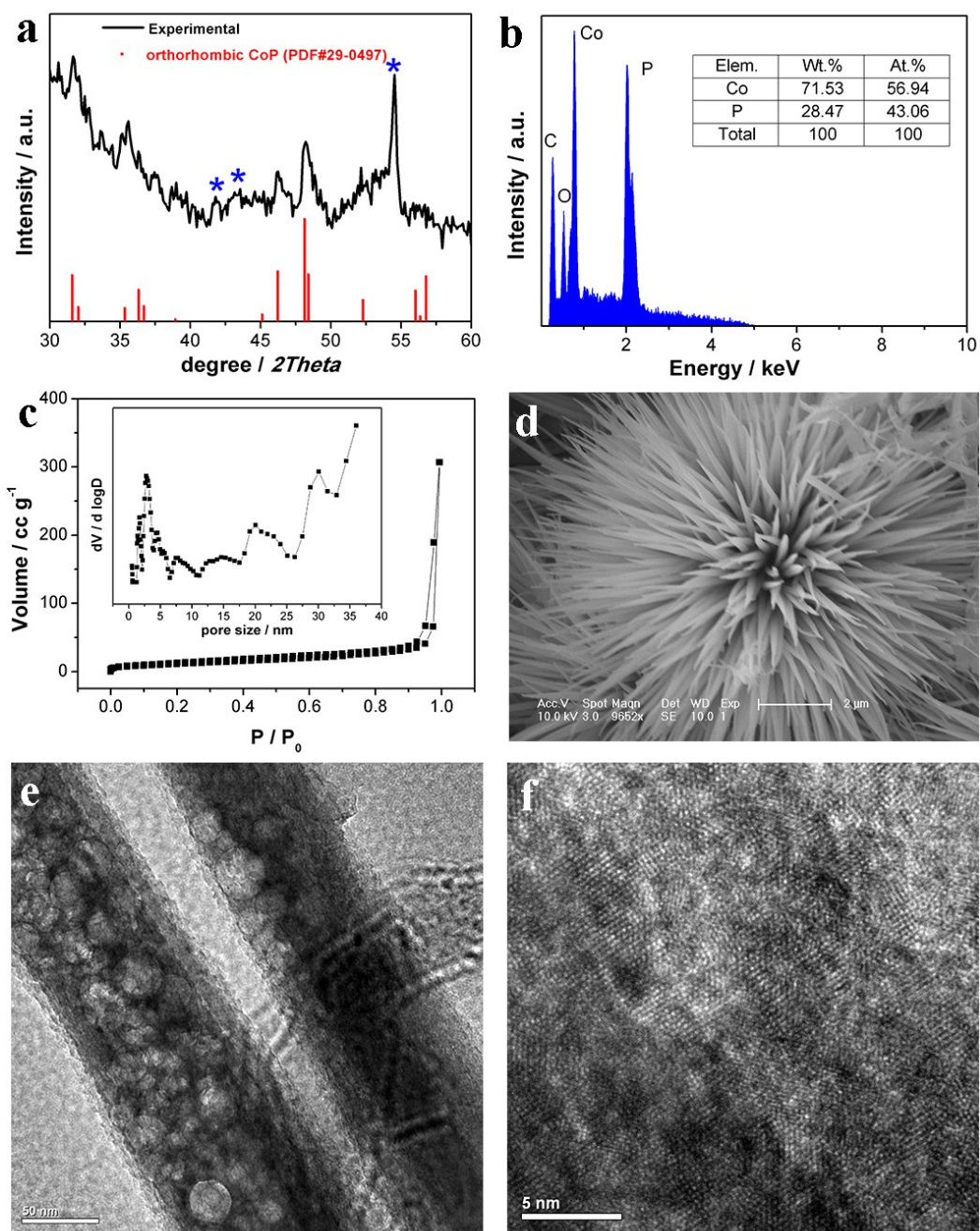
Figure S1. a) XRD patterns, peaks corresponding to graphite and carbon paper are labelled as '*'. b) EDX, c) Nitrogen adsorption/desorption isotherm plots and inset is Barrett-Joyner-Halenda (BJH) pore size distribution curves calculated from the desorption branches; d) SEM e) TEM images and f) HR-TEM of CoP nanoneedles.
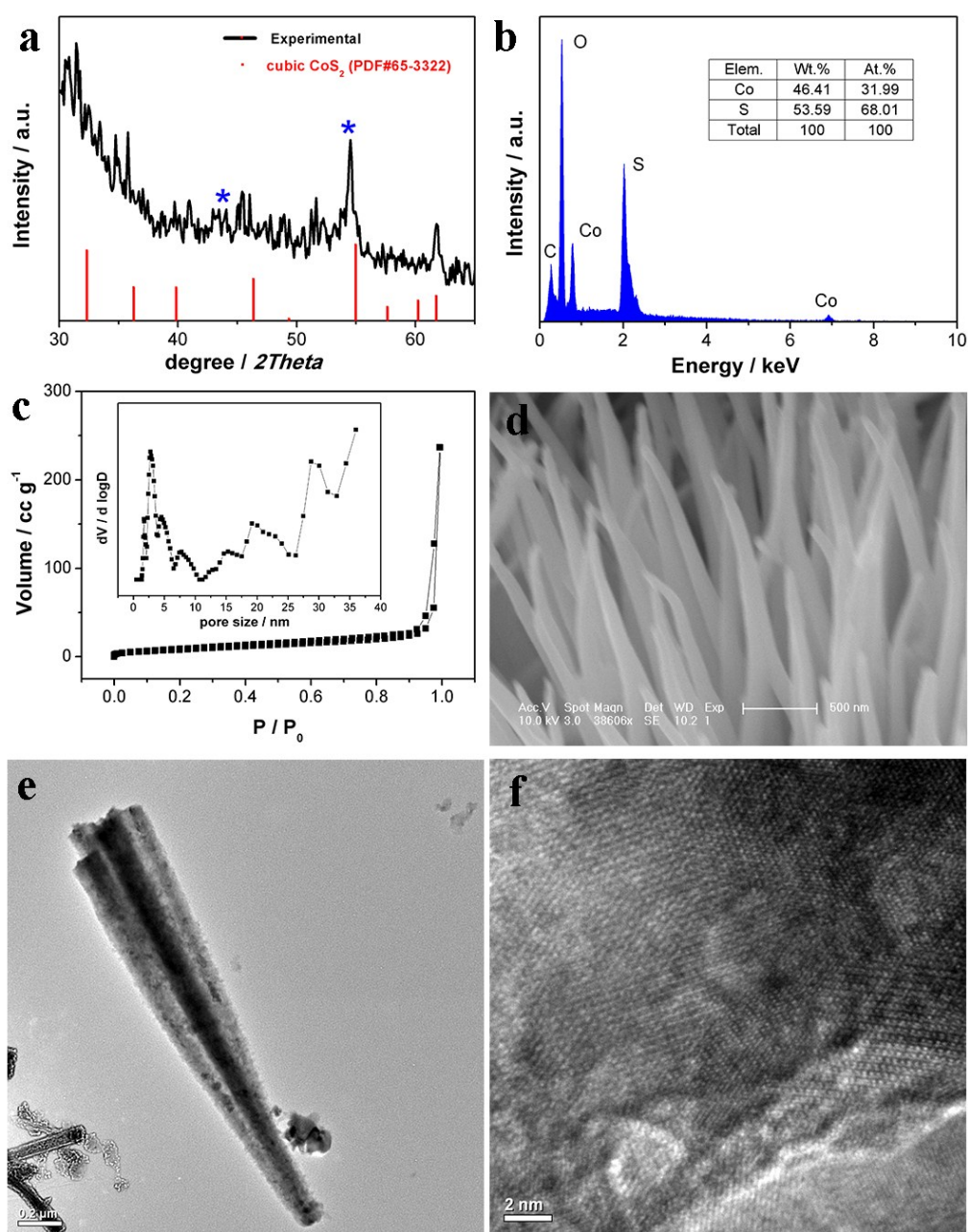
Figure S2. a) XRD patterns, peaks corresponding to graphite and carbon paper are labelled as '*'. b) EDX, c) Nitrogen adsorption/desorption isotherm plots and inset is Barrett-Joyner-Halenda (BJH) pore size distribution curves calculated from the desorption branches; d) SEM, e) TEM images and f) HR-TEM of CoS_2 nanoneedles.
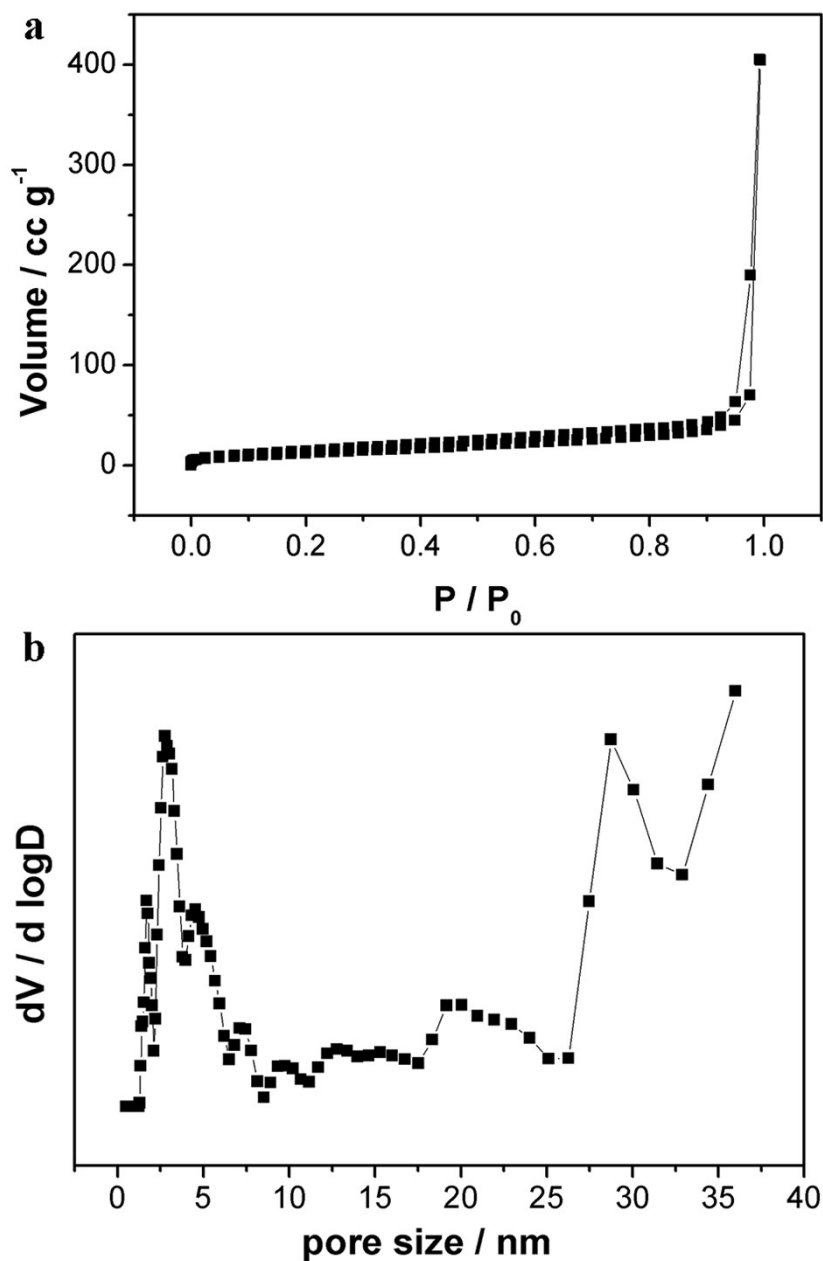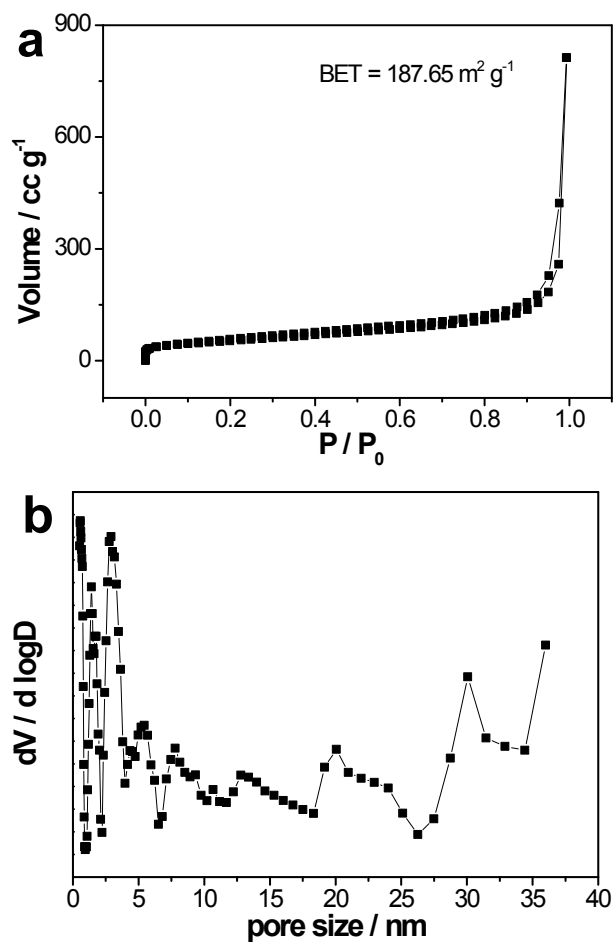
Figure S3. a) Nitrogen adsorption/desorption isotherm plots and b) Barrett-Joyner-Halenda (BJH) pore size distribution curves of CoPS calculated from the desorption branches.
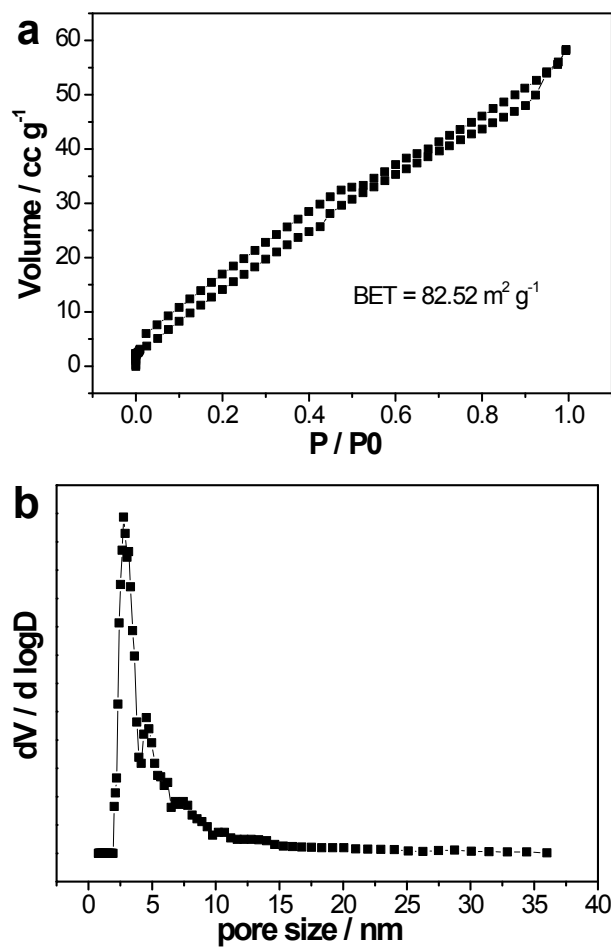
Figure S4. (a) Nitrogen adsorption/desorption isotherm plots and (b) Barrett-Joyner-Halenda (BJH) pore size distribution curves of bare carbon paper calculated from the desorption branches.

Figure S5. (a) Nitrogen adsorption/desorption isotherm plots and (b) Barrett-Joyner-Halenda (BJH) pore size distribution curves of commercial Pt/C (20%) calculated from the desorption branches.
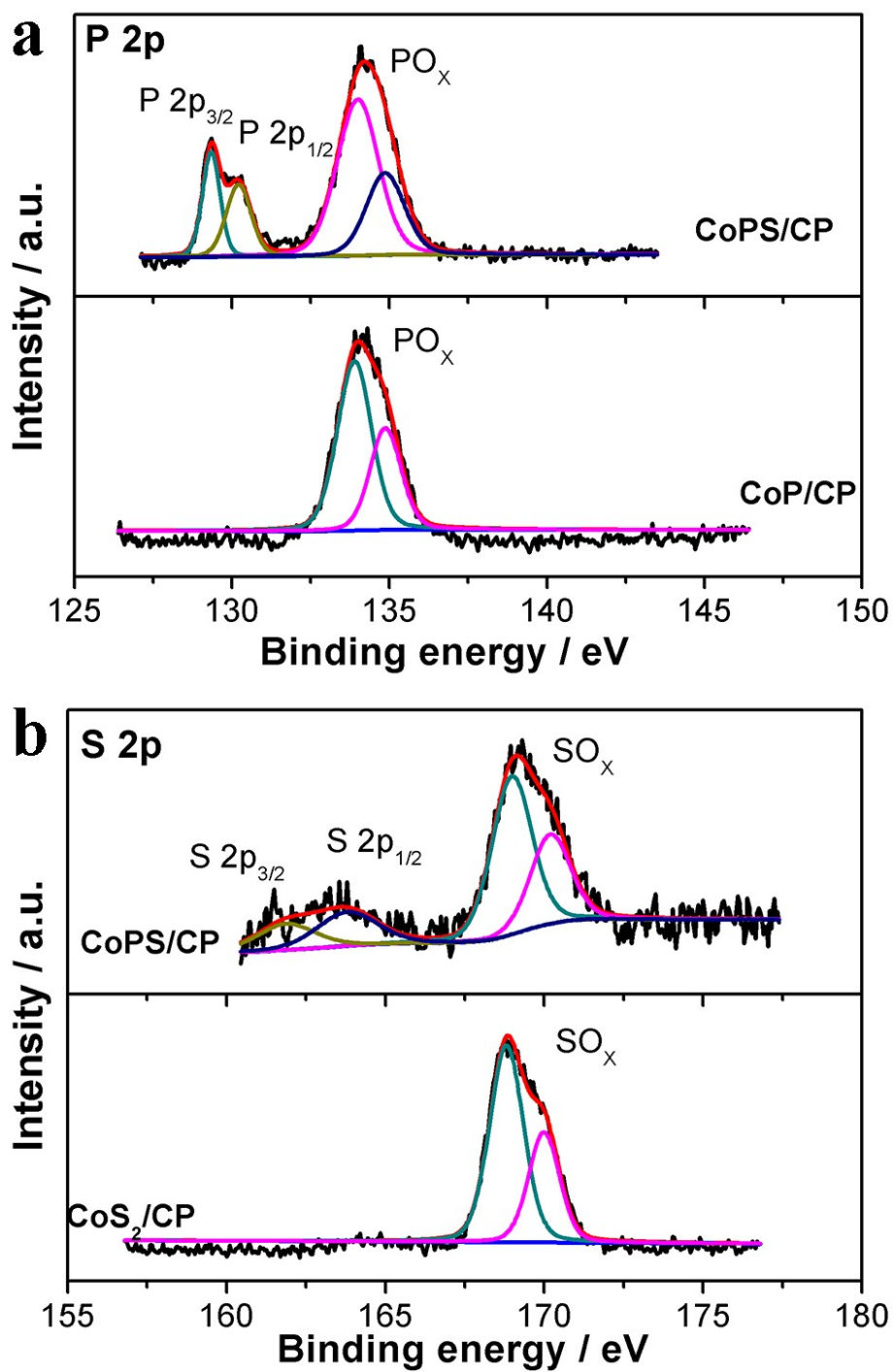
Figure S6. XPS spectroscopy of a) P and b) S of CoPS, CoP and CoS_2 scraped off the carbon paper.
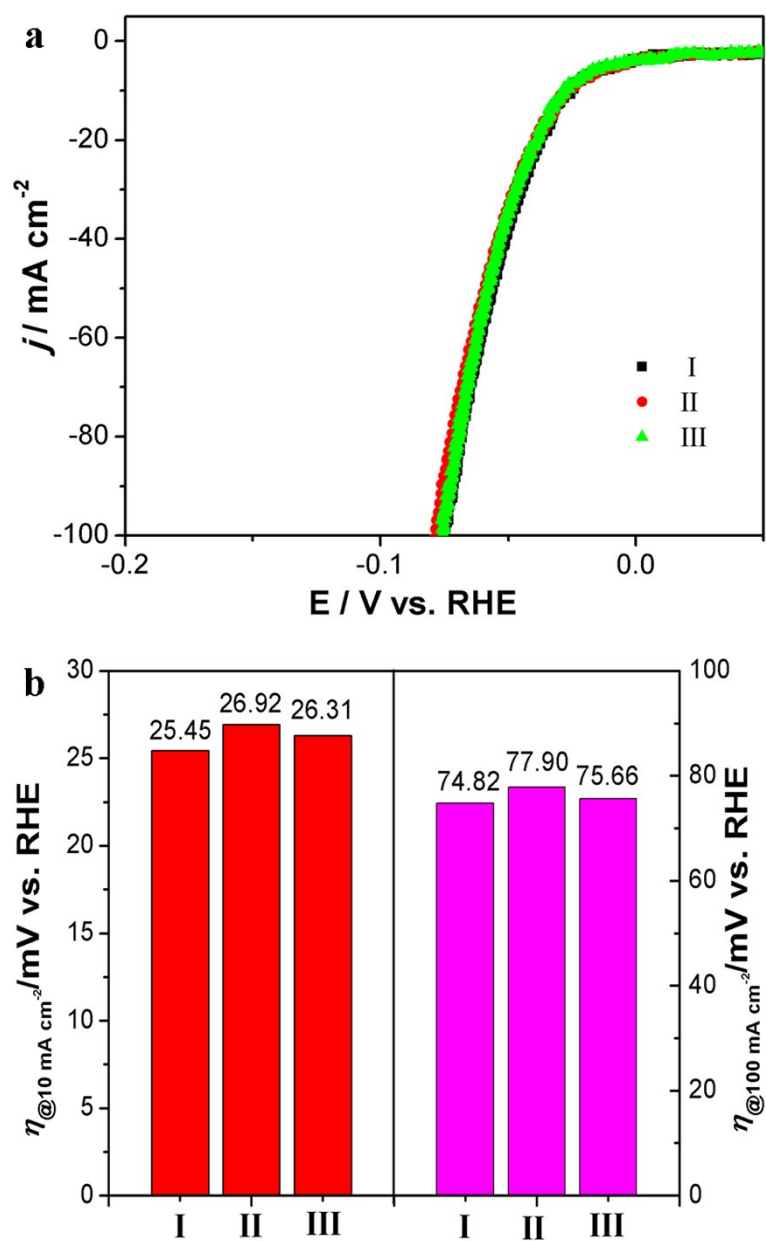
Figure S7. a) HER performance for CoPS/CP in Ar-saturated 0.5 M H_2SO_4 solution. The scan rate was 5 mV s^{-1}. I, II and III represent three independent measurements respectively; b) The Over-potential required for j =10 mA cm^{-2} and 100 mA cm^{-2}. The mass loading of CoPS on carbon paper is 0.2 mg cm^{-2}, data were corrected with 90% iR potential drop.
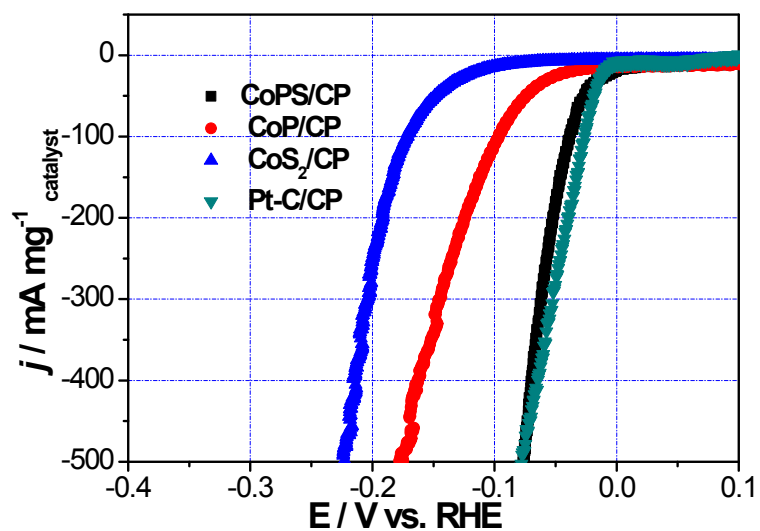
Figure S8. Polarization curves of CoPS/CP, CoP/CP, CoS$_2$/CP and Pt-C/CP. Current density is normalized to the mass of catalyst. The mass loading of CoPS, CoP, CoS$_2$ and Pt/C on carbon paper is 0.2 mg cm^{-2}, data were corrected with 90% iR potential drop.
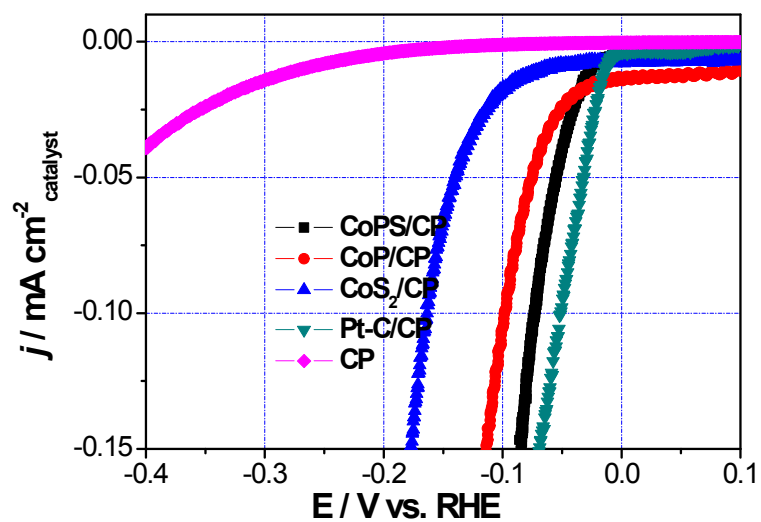
Figure S9. Polarization curves of CoPS/CP, CoP/CP, CoS$_2$/CP and Pt-C/CP. Current density is normalized to the ECSA. The mass loading of CoPS, CoP, CoS$_2$ and Pt/C on carbon paper is 0.2 mg cm^{-2}, data were corrected with 90% iR potential drop.
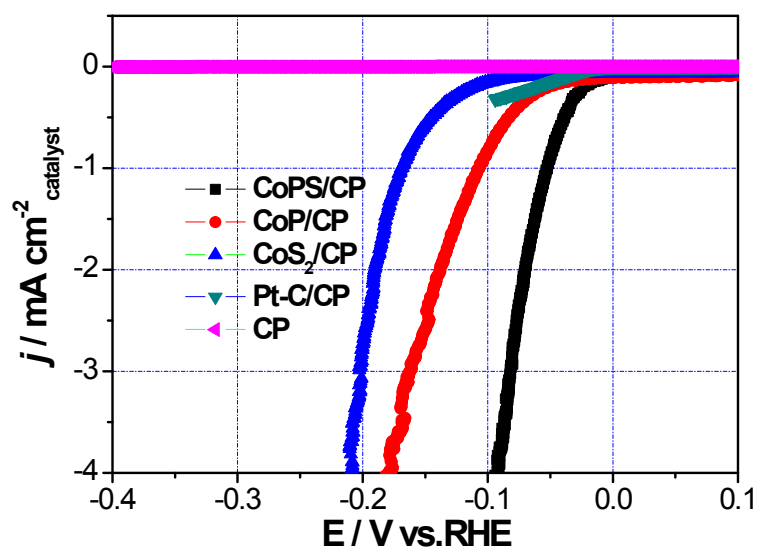
Figure S10. Polarization curves of CoPS/CP, CoP/CP, CoS$_2$/CP and Pt-C/CP. Current density is normalized to the SSAs. The mass loading of CoPS, CoP, CoS$_2$ and Pt/C on carbon paper is 0.2 mg cm^{-2}, data were corrected with 90% iR potential drop.

To compare the activity of different samples, the current is further normalized to mass current density (Figure S8), electrochemical active surface area current density (Figure S9), and Brunauer-Emmett-Teller (BET) specific surface areas (SSAs) current density (Figure S10). It can be seen clearly from Figure S8 and Figure S9, no matter current density is normalized to the mass specific activity or ECSA activity, the current density of CoPS/CP is very close to Pt-C/CP with same order of magnitude at any over-potential. However, when the current density is normalized to SSAs, as shown in Figure S10, the performance of CoPS/CP is much better than Pt-C/CP due to the high SSAs of Pt-C/CP possessed. Thus, we can say that CoPS/CP has impressive intrinsic activity for hydrogen evolution reaction.
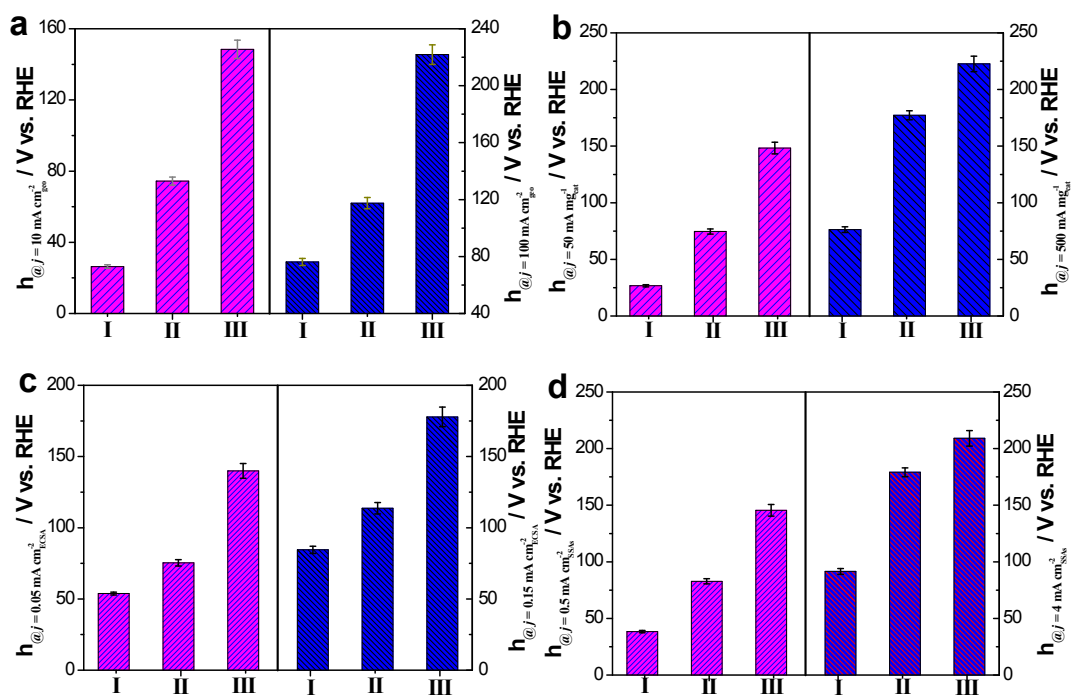
Figure S11. Overpotential required for (a) j = 10 mA cm$_{geo}^{-2}$ and j = 100 mA cm$_{geo}^{-2}$; (b) j = 50 mA mg$_{cat}^{-2}$ and j = 500 mA mg$_{cat}^{-2}$; (c) j = 0.05 mA cm$_{ECSA}^{-2}$ and j = 0.15 mA cm$_{ECSA}^{-2}$; (d) j = 0.5 mA cm$_{SSAs}^{-2}$ and j = 4 mA cm$_{SSAs}^{-2}$. 'geo' represent electrode geometric area, 'cat' represent catalyst mass, 'ECSA' represent the electrochemical active surface area, 'SSAs' represent the Brunauer-Emmett-Teller (BET) specific surface areas (SSAs). I, II and III represent CoPS/CP, CoP/CP and CoS$_2$/CP, respectively; the error bar represents the range of results from three independent measurements. The mass loading of CoPS, CoP and CoS$_2$ on carbon paper is 0.2 mg cm^{-2}, data were corrected with 90% iR potential drop.
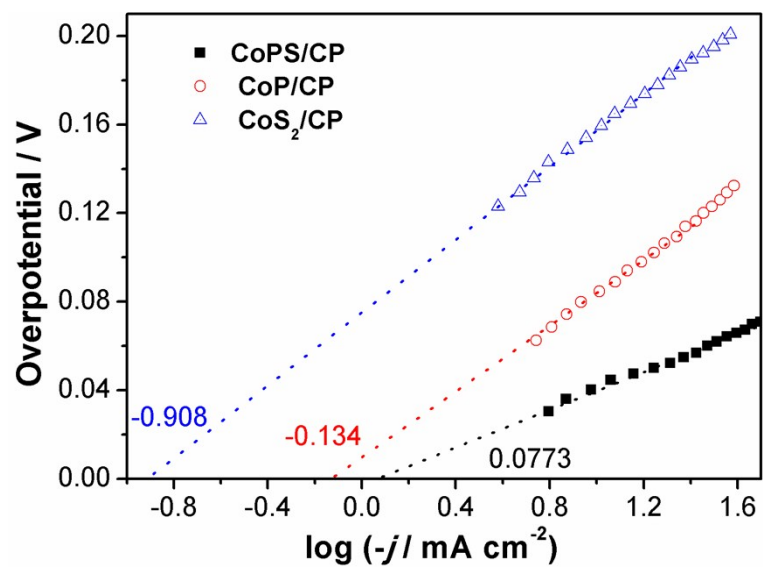
Figure S12. Tafel plots used for calculating exchange current density of CoPS/CP, CoP/CP and CoS₂/CP by extrapolation method.
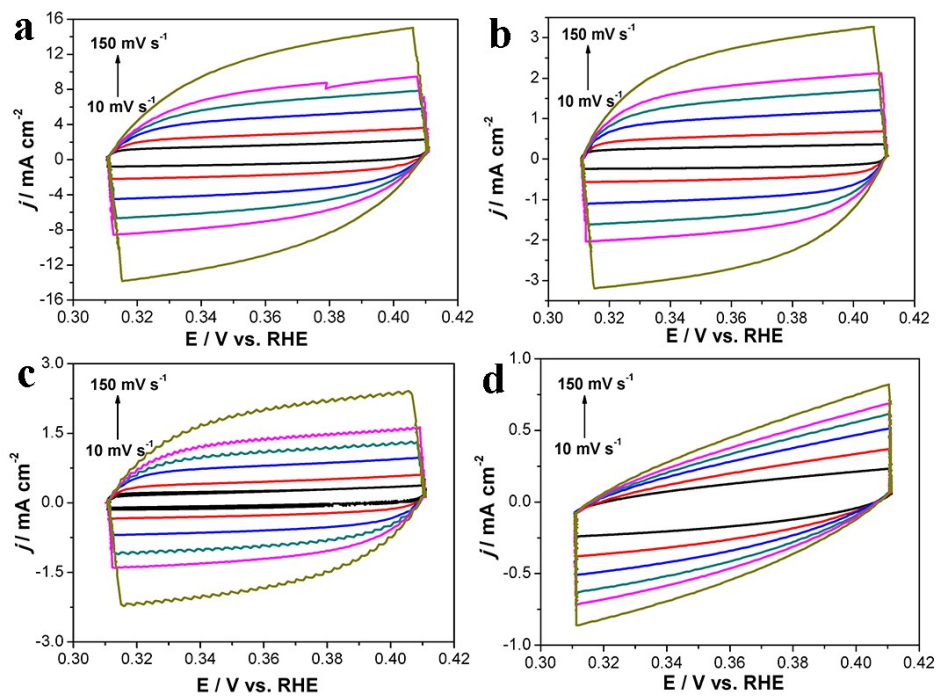
Figure S13. Scan-rate dependent CVs of a) CoPS/CP; b) CoP/CP, c) CoS$_2$/CP and d) bare CP at potential of 0.31 V~0.41 V in 0.5 M H$_2$SO$_4$. The mass loading of CoPS, CoP and CoS$_2$ on carbon paper is 0.2 mg cm^{-2}.
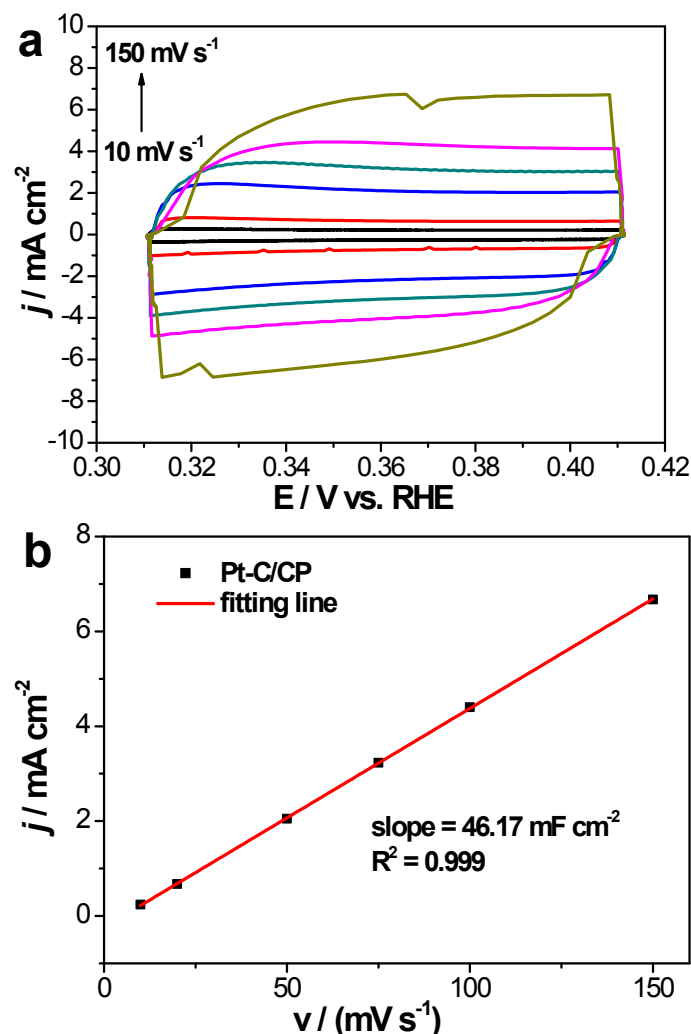
Figure S14. (a) Scan-rate (10, 25, 50, 75, 100 and 150 mV s^{-1}) dependent CVs of commercial Pt/C (20%) at potential of 0.31 V~0.41 V in 0.5 M H$_2$SO$_4$ and (b) the corresponding capacitive currents at 0.36 V as a function of scan rate. The mass loading of Pt/C (20%) on carbon paper is 0.2 mg cm^{-2}.

Electrochemical active surface area

The capacitive currents are measured in a potential range where no faradic processes are observed. We sweep the potential between 0.31 to 0.41 V vs RHE of six different scan rates (10, 25, 50, 75, 100 and 150 mV s^{-1}). The differences in current density variation ($\Delta j = j_a - j_c$) at the potential of 0.36 V vs RHE plotted against scan rate are fitted to estimate the electrochemical double-layer capacitances (C$_{dl}$), which can be used to estimate the electrochemical surface area (ECSA). The electrochemical active surface area is calculated from the following formula:

$$A_{ECSA} = \frac{specific\ capacitance}{40\ \mu F\ cm^{-2}\ per\ cm^2_{ECSA}}$$

Calculated electrochemical active surface area.

CoPS/CP: $A_{ECSA}^{CoPS} = \dfrac{72.8\ mF\ cm^{-2}}{40\ \mu F\ cm^{-2}\ per\ cm^2_{ECSA}} = 1820\ cm^{-2}_{ECSA}$

CoP/CP: $A_{ECSA}^{CoP} = \dfrac{16.7\ mF\ cm^{-2}}{40\ \mu F\ cm^{-2}\ per\ cm^2_{ECSA}} = 418\ cm^{-2}_{ECSA}$

$$\text{CoS}_2\text{/CP: } A_{\text{ECSA}}^{CoS_2} = \frac{12.6 \ mF \ cm^{-2}}{40 \ \mu F \ cm^{-2} \ per \ cm^2_{\text{ECSA}}} = 314 \ cm^{-2}_{\text{ECSA}}$$

$$\text{Pt/C: } A_{\text{ECSA}}^{Pt/C} = \frac{46.2 \ mF \ cm^{-2}}{40 \ \mu F \ cm^{-2} \ per \ cm^2_{\text{ECSA}}} = 1155 \ cm^{-2}_{\text{ECSA}} \ ;$$

Turnover Frequency Calculations.

In the calculations of the turnover frequency (TOF), we assume 40 μF cm^{-2} for the specific capacitance. TOF is calculated from the following formula:

$$\text{TOF} = \frac{\text{number of total hydrogen turnovers / cm}^{-2} \text{ of geometric area}}{number \text{ of active sites / cm}^{-2} \text{ of geometric area}}$$

The total number of hydrogen turn overs was calculated from the current density according to:

$$No. \ of \ H_2 = \left(j \frac{mA}{cm^2} \right) \left(\frac{1 \ C \ s^{-1}}{1000 \ mA} \right) \left(\frac{1 \ mol \ e^-}{96485.3 \ C} \right) \left(\frac{1 \ mol \ H_2}{2 \ mol \ e^-} \right) \left(\frac{6.022 \times 10^{23} \ H_2 \ molecules}{1 \ mol \ H_2} \right) = 3.12 \times 10^{15} \ \frac{H_2 \ / \ s}{cm^2} \ per \ \frac{mA}{cm^2}$$

Since the exact hydrogen binding site is not known, we estimate the number of active sites as the number of surface sites (including Co, P and S atoms as possible active sites) from the unit cell (see Figure S15).

The active sites per real surface area is calculated from the following formula:

$$No. \ of \ active \ sites = \left(\frac{No. \ of \ atoms \ / \ unit \ cell}{Volume \ / \ unit \ cell} \right)^{\frac{2}{3}}$$

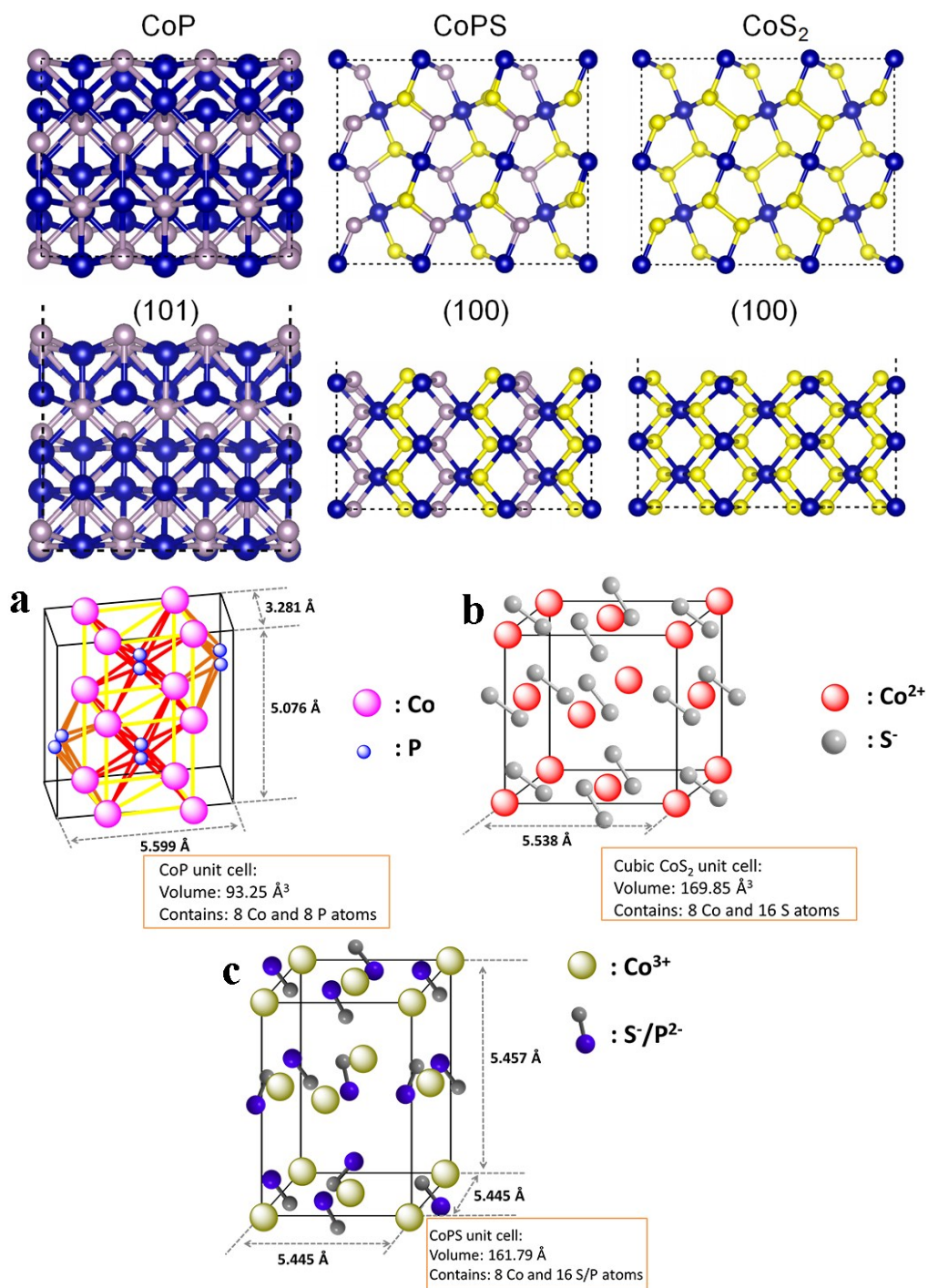From Figure S15, the number of active sites per real surface area for each phase can be calculated as follow:

$$\text{No. of active sites (CoP)} = \left(\frac{16 \ atoms \ / \ unit \ cell}{93.25 \ \mathring{A}^3 \ / \ unit \ cell} \right)^{\frac{2}{3}} = 3.09 * 10^{15} \text{ atoms cm}^2;$$

$$\text{No. of active sites (CoS}_2\text{)} = \left(\frac{24 \ atoms \ / \ unit \ cell}{169.85 \ \mathring{A}^3 \ / \ unit \ cell} \right)^{\frac{2}{3}} = 2.71 * 10^{15} \text{ atoms cm}^2;$$

$$\text{No. of active sites (CoPS)} = \left(\frac{24 \ atoms \ / \ unit \ cell}{161.79 \ \mathring{A}^3 \ / \ unit \ cell} \right)^{\frac{2}{3}} = 2.80 * 10^{15} \text{ atoms cm}^2.$$

Finally, the plot of current density can be converted into a TOF plot according to the following formula:

$$\text{TOF} = \frac{\left(3.12 \times 10^{15} \ \frac{H_2 \ / \ s}{cm^2} \ per \ \frac{mA}{cm^2} \right) \times |j|}{Nb. \ of \ active \ sites \times A_{ECSA}}$$

Figure S15. Ball-and-stick model and unit cells of CoP, CoS_2 and CoPS.

a

j / mA cm⁻² vs Potential / V vs. RHE

from the 1ˢᵗ cycle to the 3000ᵗʰ cycles

b

from the 1ˢᵗ cycle to the 3000ᵗʰ cycles
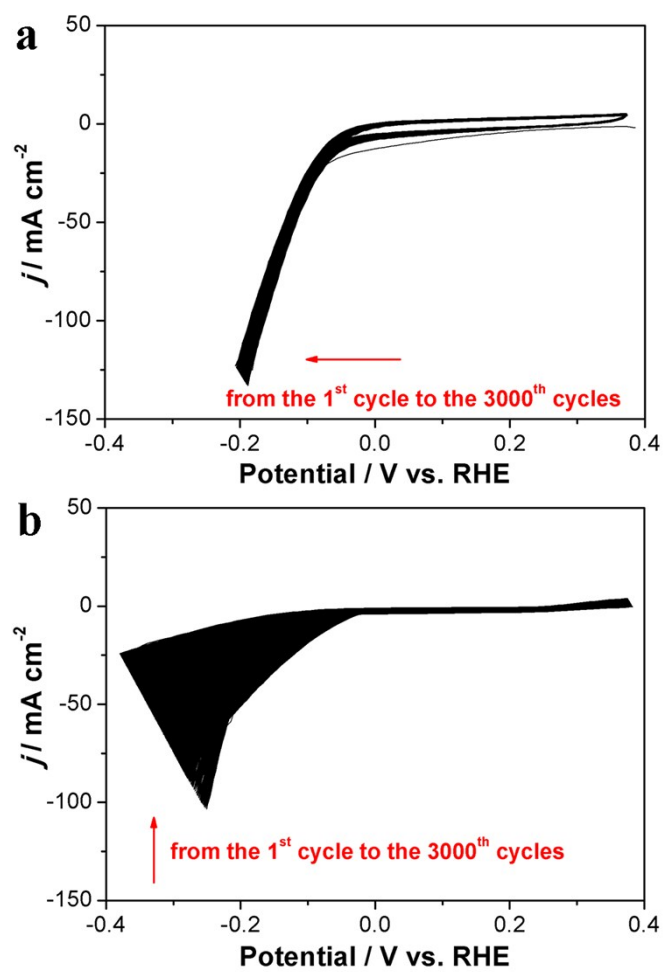
Figure S16. Cyclic voltammery curves of the complete 3000 cycles of the stability test at a scan rate of 100 mV s^{-1} in 0.5 M H_2SO_4. a) for CoP/CP and b) for CoS_2/CP.
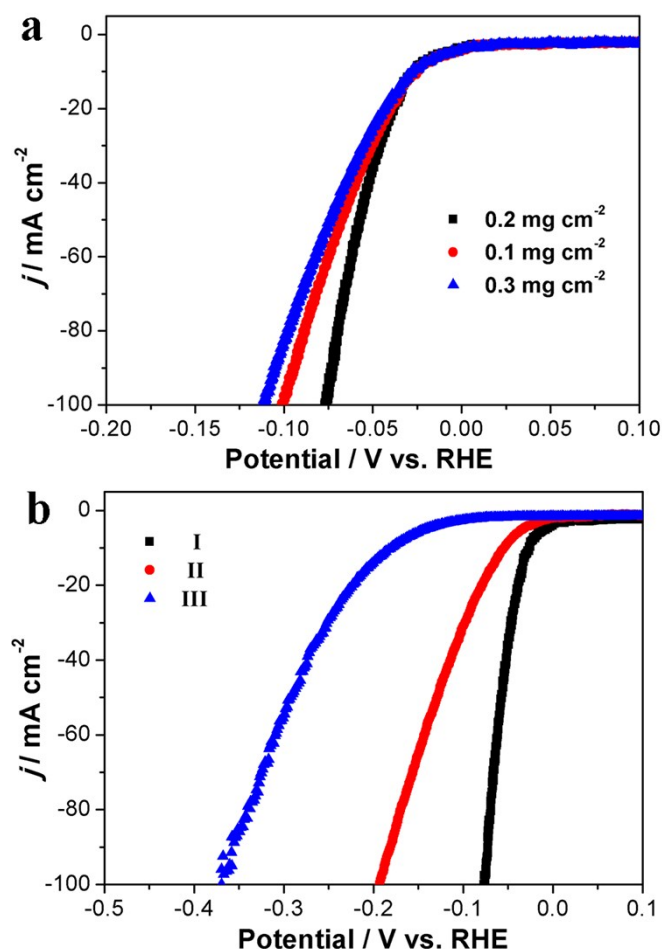
Figure S17. a) Polarization curves of CoPS/CP with different CoPS loading on carbon paper; b) Polarization curves of (I) CoPS/CP, (II) CoPS scratched down from CP and (III) direct growth without CP. Condition: Ar saturated 0.5 M H_2SO_4, scan rate was 5 mV s^{-1}.

It is important to note that the catalyst loading on carbon paper has extremely high influence on the HER activities of the catalysts. Hence, we investigated the loading effect of CoPS through varing the content of precursors used, thus acquired differed loadings at ca. 0.1 and 0.3 mg cm^{-2} on carbon paper. As shown in Figure S17a, CoPS/CP with loading of 0.1 and 0.3 mg cm^{-2} reach a current density of 100 mA cm^{-2} at overpotentials of only 101.3 and 111.5 mV, respectively. Although the performance is not as good as that of loading at 0.2 mg cm^{-2} (76.8 mV), it is still much better than most reported non-precious metal catalysts. The reason for the loading effect is explained as follows: the electrochemical HER is a surface reaction, the lower loading of catalyst on electrode surface results in fewer accessible catalytic active sites; however, the higher catalyst loading inhibits the mass transfer process during the electrochemical reaction. Thus, the loading of ~0.2 mg cm^{-2} is found as the optimum loading. The role of carbon paper substrate is elucidated through either scratching off CoPS from carbon paper and dispensed on glass carbon electrode at the same loading or directly synthesizing CoPS without the presence of carbon paper (Figure S17b). For both routes, much poorer HER performance was obtained, with overpotential of η_{100} at 194 mV and 372 mV, respectively. The above results indicate the great enhancing effect of carbon paper on promoting the electron transfer process, apart from the fact that it also acts as a rigid substrate.[6] Besides, a series of CoP$_x$S$_{2-x}$/C (x=0.5, 0.66, 1, 1.34 and 1.5; when x=1, CoPS/CP was obtained) with catalyst loading of ~0.2 mg cm^{-2} were also prepared through

adjusting the ratio of P and S precursors. The linear sweep voltammetry (LSV, Figure S18a) and the corresponding Tafel curves (Figure S18b) of CoP_xS_{1-x}/C in 0.5 M H_2SO_4 are shown in Figure S18. All these CoP_xS_{2-x}/C catalysts exhibit excellent performance towards HER, with CoPS/CP possesses the best activity as well as the smallest Tafel slope (Figure S18c and Figure S18d).
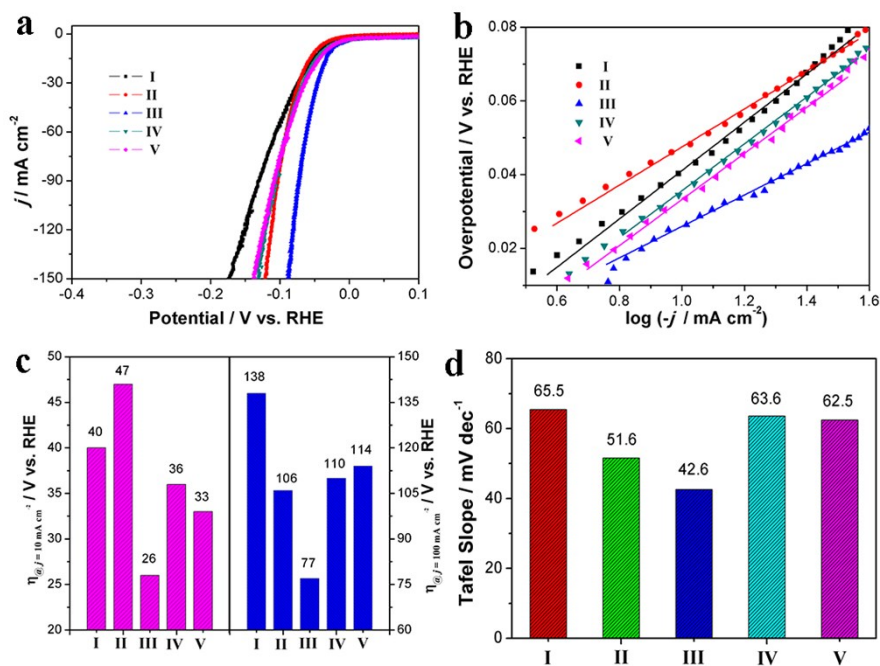
Figure S18. a) Polarization curves and b) Tafel curves of CoP_xS_{2-x}/C (x=0.5, 0.66, 1, 1.34 and 1.5; when x=1, CoPS/CP was obtained). c) Overpotential required for j = 10 mA cm^{-2} ($\eta_{@j=10 \text{ mA cm}}^{-2}$) and j = 100 mA cm^{-2}($\eta_{@j=100 \text{ mA cm}}^{-2}$); d) Tafel slope of different catalysts; I, II, III IV and V in (a)-(d) represents $CoP_{0.5}S_{1.5}/C$, $CoP_{0.66}S_{1.34}/C$, CoP_1S_1/C, $CoP_{1.34}S_{1.66}/C$ and $CoP_{1.5}S_{0.5}/C$, respectively.

Table S1. BET surfaces area (S_{BET}), ECSAs and Cdl of CoPS, CoP, CoS$_2$, carbon paper (#60, Fuel Cell Earth) and commercial Pt/C (20wt %) samples.

Samples	S_{BET} (m^2 g^{-1})	ECSAs (cm^{-2})	Cdl (mF cm^{-2})
CoPS/CP	20.41	1820	145.6
CoP/CP	13.25	418	33.4
CoS$_2$/CP	9.12	314	25.1
Carbon paper	82.52	42.5	1.71
Commercial Pt/C (20wt%)	187.65	1155	46.17

Table S2. HER performances of CoPS/CP and other reported electrocatalysts in 0.5 M H_2SO_4.
('-' represent the value was un-given in Reference).

Catalysts	Onset potential	Overpotential @ 10 mA cm^{-2}	Overpotential @ 100 mA cm^{-2}	Tafel slope mV dec^{-1}	Exchange current density (mA cm^{-2})	Ref.
Pt/C (20%)	0	14.2	33.7	29.9	1.19	This work
CoPS/CP	**4**	**25.9**	**76.8**	**42.6**	**0.81**	
CoP/CP	41.1	74.3	177.8	78.9	0.73	
CoS$_2$/CP	84.4	148.3	222.4	77.7	0.12	
pyrite CoPS film	-	128	-	48	0.056	4
pyrite CoPS NW	-	61	-	65	0.554	
pyrite CoPS NPl	-	48	-	57	0.984	
CoS|P/CNT	-	48	109	55	1.14	7
Fe$_{0.5}$Co$_{0.5}$P/CC	-	37	98	30	-	3
NiCo$_2$P$_x$	-	104	-	59.6	-	8
CoMoS$_3$ hollow prism	75	171	-	56.9	0.011	9
Fe$_{0.9}$Co$_{0.1}$S$_2$/CNT	-	105	-	46	-	10
Mn$_{0.05}$Co$_{0.95}$Se$_2$	174	195	-	36	0.0683	11
np-(Co$_{0.52}$Fe$_{0.48}$)$_2$P	12	64	-	44	0.5	12
Co$_9$S$_8$@MoS$_2$/CNFs	64	190	-	110	-	13
CoP/CC	38	67	204	51	0.288	14
CoP/CNT	40	122	-	54	0.13	15
CoP/Ti	-	75	-	50	0.14	16
MoS$_2$/CoSe$_2$	11	68	-	36	0.073	17
CoS$_2$ NW	~75	145	~220	51.6	0.0151	18
CoS$_2$ film		190	-	51.4	1.97×10^{-3}	
CoS$_2$ MW		158	~240	58	0.0188	
CoS$_2$/RGO-CNT	-	142	178	51	0.0625	19
CoSe$_2$ NP/CP	-	139	184	42.1	$(4.9 \pm 1.4) \times 10^{-3}$	20
CoSe$_2$ nanobelts	50	-	-	48	8.4×10^{-3}	21
Co-NRCNTs	50	260	-	69	0.01	22

Table S3. HER performances of CoPS/CP and other reported electrocatalysts in 1 M KOH.

Catalysts	Overpotential @ 10 mA cm^{-2}	Overpotential @ 100 mA cm^{-2}	Tafel slope mV dec^{-1}	Reference
CoPS/CP	107	207	88.3	This work
NiCo$_2$P$_x$	58	127	34.3	[23]
np-(Co$_{0.52}$Fe$_{0.48}$)$_2$P	79	180	40	[12]
CoP/CC	209	500	129	[14]
Co-NRCNTs	370	-	-	[22]
Ni$_{0.33}$Co$_{0.67}$S$_2$	88	-	118	[24]
Ni/NiP	130	-	58.5	[25]
Ni/NiS	230	-	123.3	
Ni$_3$S$_2$/NF	223	-	123.3	[23]
Ni$_{12}$P$_5$/Ni$_3$ (PO$_4$)$_2$-HS	114	-	93.1	[26]
CoP NS	111	-	124.5	[27]

Reference

(1)	Perdew, J. P.; Burke, K.; Ernzerhof, M. *Phys. Rev. Lett.* **1996**, *77*, 3865.

(2)	Kresse, G.; Furthmuller, J. *Phys. Rev. B* **1996**, *54*, 11169.

(3)	Tang, C.; Gan, L.; Zhang, R.; Lu, W.; Jiang, X.; Asiri, A. M.; Sun, X.; Wang, J.; Chen, L. *Nano letters* **2016**, *16*, 6617.

(4)	Caban-Acevedo, M.; Stone, M. L.; Schmidt, J. R.; Thomas, J. G.; Ding, Q.; Chang, H. C.; Tsai, M. L.; He, J. H.; Jin, S. *Nat Mater* **2015**, *14*, 1245.

(5)	Zheng, Y.; Jiao, Y.; Zhu, Y.; Li, L. H.; Han, Y.; Chen, Y.; Du, A.; Jaroniec, M.; Qiao, S. Z. *Nat. Commun.* **2014**, *5*, 3783.

(6)	Wu, R.; Zhang, J.; Shi, Y.; Liu, D.; Zhang, B. *J. Am. Chem. Soc.* **2015**, *137*, 6983.

(7)	Liu, W.; Hu, E.; Jiang, H.; Xiang, Y.; Weng, Z.; Li, M.; Fan, Q.; Yu, X.; Altman, E. I.; Wang, H. *Nat. Commun.* **2016**, *7*, 10771.

(8)	Zhang, R.; Wang, X.; Yu, S.; Wen, T.; Zhu, X.; Yang, F.; Sun, X.; Wang, X.; Hu, W. *Adv. Mater.* **2016**, 1605502.

(9)	Yu, L.; Xia, B. Y.; Wang, X.; Lou, X. W. *Adv. Mater.* **2016**, *28*, 92.

(10)	Wang, D.-Y.; Gong, M.; Chou, H.-L.; Pan, C.-J.; Chen, H.-A.; Wu, Y.; Lin, M.-C.; Guan, M.; Yang, J.; Chen, C.-W.; Wang, Y.-L.; Hwang, B.-J.; Chia-Chun Chen; Dai, a. H. *J. Am. Chem. Soc.* **2015**, *137*, 1587.

(11)	Liu, Y.; Hua, X.; Xiao, C.; Zhou, T.; Huang, P.; Guo, Z.; Pan, B.; Xie, Y. *J. Am. Chem. Soc.* **2016**, *138*, 5087.

(12)	Tan, Y.; Wang, H.; Liu, P.; Shen, Y.; Cheng, C.; Hirata, A.; Fujita, T.; Tang, Z.; Chen, M. *Energy Environ. Sci.* **2016**, *9*, 2257.

(13)	Zhu, H.; Zhang, J.; Yanzhang, R.; Du, M.; Wang, Q.; Gao, G.; Wu, J.; Wu, G.; Zhang, M.; Liu, B.; Yao, J.; Zhang, X. *Adv. Mater.* **2015**, *27*, 4752.

(14)	Tian, J.; Liu, Q.; Asiri, A. M.; Sun, X. *J. Am. Chem. Soc.* **2014**, *136*, 7587.

(15)	Liu, Q.; Tian, J.; Cui, W.; Jiang, P.; Cheng, N.; Asiri, A. M.; Sun, X. *Angew. Chem. Int. Ed.* **2014**, *53*, 6710.

(16)	Popczun, E. J.; Read, C. G.; Roske, C. W.; Lewis, N. S.; Schaak, R. E. *Angew. Chem. Int. Ed.* **2014**, *126*, 5531.

(17)	Gao, M. R.; Liang, J. X.; Zheng, Y. R.; Xu, Y. F.; Jiang, J.; Gao, Q.; Li, J.; Yu, S. H. *Nat. Commun.* **2015**, *6*, 5982.

(18)	Faber, M. S.; Dziedzic, R.; Lukowski, M. A.; Kaiser, N. S.; Ding, Q.; Jin, S. *J. Am. Chem. Soc.* **2014**, *136*, 10053.

(19)	Peng, S.; Li, L.; Han, X.; Sun, W.; Srinivasan, M.; Mhaisalkar, S. G.; Cheng, F.; Yan, Q.; Chen, J.; Ramakrishna, S. *Angew. Chem. Int. Ed.* **2014**, *53*, 12594.

(20)	Kong, D.; Wang, H.; Lu, Z.; Cui, Y. *J. Am. Chem. Soc.* **2014**, *136*, 4897.

(21)	Xu, Y. F.; Gao, M. R.; Zheng, Y. R.; Jiang, J.; Yu, S. H. *Angew. Chem. Int. Ed.* **2013**, *52*, 8546.

(22)	Zou, X.; Huang, X.; Goswami, A.; Silva, R.; Sathe, B. R.; Mikmekova, E.; Asefa, T. *Angew. Chem. Int. Ed.* **2014**, *53*, 4372.

(23)	Zhou, W.; Wu, X.-J.; Cao, X.; Huang, X.; Tan, C.; Tian, J.; Liu, H.; Wang, J.; Zhang, H. *Energy Environ. Sci.* **2013**, *6*, 2921.

(24)	Peng, Z.; Jia, D.; Al-Enizi, A. M.; Elzatahry, A. A.; Zheng, G. *Adv. Energy Mater.* **2015**, *5*, 1402031.

(25)	Chen, G.-F.; Ma, T. Y.; Liu, Z.-Q.; Li, N.; Su, Y.-Z.; Davey, K.; Qiao, S.-Z. *Adv. Funct. Mater.* **2016**, *26*, 3314.

(26)	Chang, J.; Lv, Q.; Li, G.; Ge, J.; Liu, C.; Xing, W. *Appl. Catal. B: Environ.* **2017**, *204*, 486.

(27)	Chang, J.; Liang, L.; Li, C.; Wang, M.; Ge, J.; Liu, C.; Xing, W. *Green Chem.* **2016**, *18*, 2287.